Impact of oceanic circulation on biological carbon storage in the ocean and atmospheric pCO_2

I. Marinov,[1,2] A. Gnanadesikan,[3] J. L. Sarmiento,[4] J. R. Toggweiler,[3] M. Follows,[1] and B. K. Mignone[5]

Received 8 February 2007; revised 15 February 2008; accepted 6 March 2008; published 23 July 2008.

[1] We use both theory and ocean biogeochemistry models to examine the role of the soft-tissue biological pump in controlling atmospheric CO_2. We demonstrate that atmospheric CO_2 can be simply related to the amount of inorganic carbon stored in the ocean by the soft-tissue pump, which we term (OCS_{soft}). OCS_{soft} is linearly related to the inventory of remineralized nutrient, which in turn is just the total nutrient inventory minus the preformed nutrient inventory. In a system where total nutrient is conserved, atmospheric CO_2 can thus be simply related to the global inventory of preformed nutrient. Previous model simulations have explored how changes in the surface concentration of nutrients in deepwater formation regions change the global preformed nutrient inventory. We show that changes in physical forcing such as winds, vertical mixing, and lateral mixing can shift the balance of deepwater formation between the North Atlantic (where preformed nutrients are low) and the Southern Ocean (where they are high). Such changes in physical forcing can thus drive large changes in atmospheric CO_2, even with minimal changes in surface nutrient concentration. If Southern Ocean deepwater formation strengthens, the preformed nutrient inventory and thus atmospheric CO_2 increase. An important consequence of these new insights is that the relationship between surface nutrient concentrations, biological export production, and atmospheric CO_2 is more complex than previously predicted. Contrary to conventional wisdom, we show that OCS_{soft} can increase and atmospheric CO_2 decrease, while surface nutrients show minimal change and export production decreases.

Citation: Marinov, I., A. Gnanadesikan, J. L. Sarmiento, J. R. Toggweiler, M. Follows, and B. K. Mignone (2008), Impact of oceanic circulation on biological carbon storage in the ocean and atmospheric pCO_2, *Global Biogeochem. Cycles*, *22*, GB3007, doi:10.1029/2007GB002958.

1. Introduction

[2] *Volk and Hoffert* [1985] define an ocean carbon pump as "a process that depletes the ocean surface of dissolved inorganic carbon (*DIC*) relative to the deep-water *DIC*." They recognized three such pumps: the soft-tissue pump, the carbonate pump and the solubility pump. While the first two are biological, the third is a response to solubility differences of CO_2 in warm and cold water. Of the three, the soft-tissue or organic pump receives the most attention because it is potentially the largest and also seems to exhibit the most variability over time, e.g., glacial-interglacial cycles. Recent work suggests, however, that the biological process causing the surface to deep *DIC* difference ($DIC_{deep} - DIC_{surf}$) to vary in the real ocean is quite different from the kind of pumping process envisioned by Volk and Hoffert.

[3] Organisms create a *DIC* difference when they take up PO_4 and CO_2 at the surface and create sinking organic particles that are then remineralized back into PO_4 and CO_2 in the deep ocean. In their derivations, *Volk and Hoffert* [1985] defined the soft-tissue pump as a function of the mean oceanic vertical gradient of PO_4, i.e., $\Delta DIC = r_{C:P} \cdot \Delta PO_4$, where $r_{C:P}$ is a stoichiometric ratio. Similarly, *Broecker and Peng* [1992] and *Gruber and Sarmiento* [2002] determine the soft-tissue contribution from the difference between local and mean surface PO_4.

[4] However, as emphasized recently by *Ito and Follows* [2005] (henceforth IF), there are two components to ΔPO_4, the preformed and the remineralized components. The preformed PO_4 are the biologically unutilized nutrients which are subducted into the ocean interior. As shown in

[1]Program in Atmospheres, Oceans, and Climate, Massachusetts Institute of Technology, Cambridge, Massachusetts, USA.
[2]Now at Department of Marine Chemistry and Geochemistry, Woods Hole Oceanographic Institution, Woods Hole, Massachusetts, USA.
[3]NOAA/Geophysical Fluid Dynamics Laboratory, Princeton, New Jersey, USA.
[4]Atmospheric and Oceanic Sciences Program, Princeton University, Princeton, New Jersey, USA.
[5]The Brookings Institution, Washington, D. C., USA.

0886-6236/08/2007GB002958$12.00

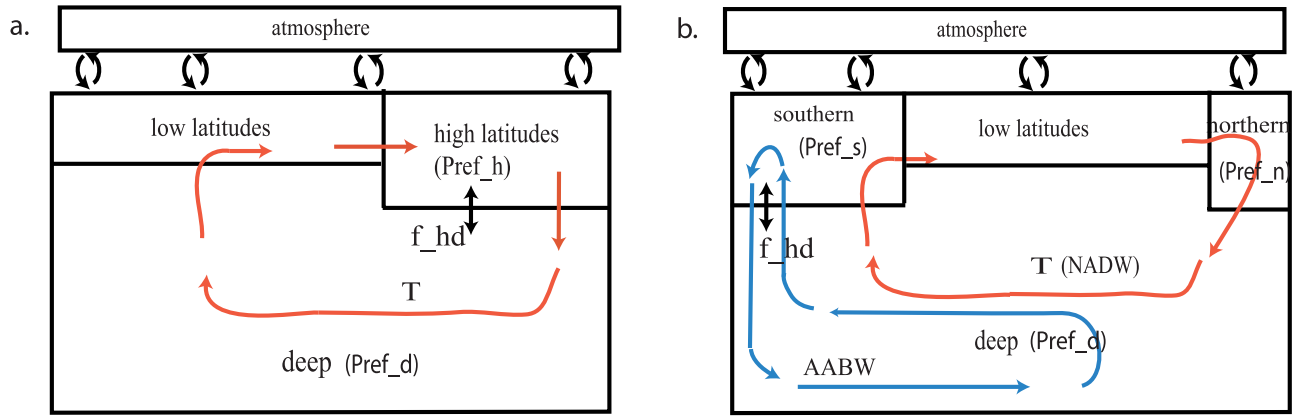

Figure 1. (a) Simplified 3BM of oceanic circulation as discussed, for example, by *Sarmiento and Toggweiler* [1984]. (b) 4BM captures the first-order processes relevant for the carbon cycle. Deep preformed PO_4, $Pref_d$, determines atmospheric pCO_2. $Pref_d$ depends on both NADW strength (represented here by T) and AABW strength (f_{hd}). Relative changes in these ventilation rates explain observed changes in atmospheric pCO_2 in our GCMs.

the three-box models of *Sarmiento and Toggweiler* [1984] *Siegenthaler and Wenk* [1984], or *Knox and McElroy* [1984], it is the preformed component, rather than the total PO_4, that is most likely to vary over time. Hence, *Volk and Hoffert*'s [1985] pump metaphor and its emphasis on fluxes of organic matter and surface-to-deep gradients of total phosphate seems to us to be pointing in the wrong direction.

[5] The preformed PO_4 in the three-box model is set in the model's polar box, which is generally taken to represent the high-PO_4 surface waters of the Southern Ocean (Figure 1a). Utilization (or underutilization) of PO_4 by organisms in the polar box can lower (or raise) the preformed PO_4 and make $DIC_{deep} - DIC_{surf}$ large (or small). However, the polar box in the three-box model is really a combination of the ocean's two areas of deepwater formation, the low-PO_4 North Atlantic and the high-PO_4 Southern Ocean. As pointed out by *Toggweiler et al.* [2003], the spread or difference in preformed PO_4 between the low-PO_4 north and the high-PO_4 south gives $DIC_{deep} - DIC_{surf}$ an additional degree of freedom to vary, and the spread owes more to the distinctive circulations in the north and south than to differences in end-member nutrient utilization. So, while it is possible for organisms to alter $DIC_{deep} - DIC_{surf}$ by changing polar PO_4 concentrations it is also possible that changes in circulation alter $DIC_{deep} - DIC_{surf}$ by changing the mix of northern and southern water that fills the ocean interior.

[6] Hence, we propose in section 3 of this paper a less biased terminology, Ocean Carbon Storage (OCS_{soft}), to describe how $DIC_{deep} - DIC_{surf}$ varies in the ocean. We also show that a theory based on the weighting of northern and southern components does an excellent job of predicting the OCS_{soft} in models with different circulations. Changes in OCS_{soft} directly affect atmospheric pCO_2. We show in section 4, along the lines of *IF*, that atmospheric pCO_2 is exponentially related to OCS_{soft} and the global inventory of preformed PO_4 at the limit where gas exchange rates are artificially fast enough to suppress ocean-atmosphere pCO_2 differences. The relationship becomes more complicated if we take into account the surface disequilibrium of CO_2 (section 5).

2. Methods: Model Simulations

[7] We perform long equilibrium simulations for eight versions of a GCM with different oceanic circulations produced by different mixing or winds. The total ocean-atmospheric carbon inventory is identical among all models. Because the partitioning of inorganic carbon between ocean and atmosphere depends on circulation, atmospheric pCO_2 at equilibrium is different in the different models.

[8] The GCM we use is the Geophysical Fluid Dynamics Laboratory Modular Ocean Model version 3 [*Pacanowski and Griffies*, 1999] with a biogeochemistry component consistent with OCMIP-2 specifications [*Najjar et al.*, 2007; R. Najjar and J. Orr, 1998, Design of OCMIP-2 simulations of chlorofluorocarbons, the solubility pump and common biogeochemistry, available at http://www.cgd.ucar.edu/oce/OCMIP/design.pdf]. New biological production is calculated by restoring surface PO_4 to the observed seasonal values $PO_{4\ obs}$ of *Louanchi and Najjar* [2000] at each time step t, whenever $PO_4 > PO_{4\ obs}$:

$$J_{prod}(x,y,z,t) = (PO_4(x,y,z,t) - PO_{4\,obs}(x,y,z,t))/\tau, \qquad (1)$$

for $z < 75\ m$; τ is the biological timescale. x, y, z are model longitude, latitude and depth. Globally integrated PO_4 is set constant in all experiments.

[9] Two sets of simulations are performed: a standard, realistic set with τ = 30 days and one with extremely inefficient biology (τ = 1 year). For simplicity we turn off the solubility and carbonate pumps by setting surface ocean temperature and salinity constant everywhere in the CO_2 gas exchange calculations, and by setting alkalinity constant everywhere. This soft-tissue model configuration was

designed by *Marinov* [2005, pp. 1–18] and used by *Marinov et al.* [2006].

[10] In addition to the standard biogeochemical tracers from previous versions of this model (O_2, PO_4, dissolved inorganic carbon (*DIC*), particulate organic phosphate, dissolved organic phosphate), we add "preformed phosphate" as a new tracer. The preformed tracer is set equal to the model PO_4 concentration at each surface ocean point. In the ocean interior the preformed tracer is advected and mixed without biological sources or sinks.

[11] Mixing is parameterized in terms of a diapycnal diffusion coefficient K_v and an isopycnal coefficient A_i. The latter coefficient is used both for along-isopycnal stirring and for representing advective fluxes associated with mesoscale eddies [*Gent and McWilliams*, 1990]. Several different model versions are designed as follows.

[12] 1. In the standard or LL model, K_v varies hyperbolically in the ocean from 0.15 cm^2/s at the surface to 1.3 cm^2/s at 5000 m with a hyperbolic tangent transition at 2500 m [*Bryan and Lewis*, 1979]. Isopycnal mixing A_i coefficient is set to 1000 m^2/s everywhere in the ocean. LL stands for low-K_v and low-A_i values.

[13] 2. In the high-K_v model, K_v varies hyperbolically from 0.6 cm^2/s at the surface to 1.3 cm^2/s at 5000 m everywhere in the ocean. A_i is set to 1000 m^2/s as above.

[14] 3. In the high-A_i model, A_i is set to 2000 m^2/s everywhere while K_v has LL model values.

[15] 4. In the high-A_i-high-K_v model, A_i is set to 2000 m^2/s everywhere while K_v is as in the high-K_v model.

[16] 5. In a high south K_v model, vertical mixing coefficient K_v is set to 1 cm^2/s throughout the water column south of 50°S. Elsewhere in the ocean, K_v has the same hyperbolical profile as the LL model. A_i is set to 1000 m^2/s everywhere as in LL.

[17] The above five models are based on *Gnanadesikan et al.* [2002, 2003, 2004] and use seasonal wind stresses of *Hellerman and Rosenstein* [1983]. Nutrient properties and DIC distributions from these models were analyzed comparatively by *Marinov* [2005, pp. 65–97].

[18] 6. To explore the effect of extreme Southern Ocean wind stress we design three other models where winds are set to *Hellerman and Rosenstein* [1983] everywhere except south of 30°S where wind stress is either increased three fold (windx3 model), increased two fold (windx2 model) or decreased by 50% (windx0.5 model) relative to the LL model (Figure 2i). K_v and A_i have LL model values. The windx2 model has wind stresses comparable to the ECMWF stresses of *Trenberth et al.* [1989].

[19] Each of the above models is run for a few thousand years to equilibrium with both regular gas exchange and fast gas exchange (where surface pCO_2 at each time step is set equal to atmospheric pCO_2 calculated at the previous time step). In an infinitely fast gas exchange scenario, CO_2 at the ocean surface is in equilibrium with the atmosphere above, and surface *DIC* disequilibrium is zero. This assumption is fundamental both in deriving theoretical models of the ocean carbon cycle (section 4.1) and making sense of model results (section 4.2–4.3). However, as we will see in section 5 and has already been pointed out by others [e.g., *Toggweiler et al.*, 2003], the surface *DIC* disequilibrium can have a sizable impact on the amount of carbon stored in the ocean, causing departures from simple theories.

[20] The standard (LL) model with fast gas exchange is run to equilibrium from an arbitrary dissolved inorganic carbon (*DIC*) distribution with a fixed preindustrial atmospheric CO_2 concentration of 278 ppm by allowing CO_2 to invade the ocean until the absolute value of the global, annual mean air-sea CO_2 flux is less than 0.01 PgC/a. This model is then run further with constant global ocean-atmospheric carbon inventory, while atmospheric CO_2 is allowed to vary. After bringing the LL model to a new equilibrium, we calculate the total inorganic carbon inventory (total ocean *DIC* plus total atmospheric CO_2). We then run simulations for all other circulation models while keeping the total ocean-atmosphere carbon inventory constant and identical with the LL inventory. Since this inventory is kept constant, atmospheric pCO_2 is different between simulations with different physical models, as well as between fast and regular gas exchange simulations in the same physical model.

3. Model Results

[21] The present section discusses results from equilibrium simulations using the eight different models described above. We show that export production and surface nutrients are not good indicators for atmospheric pCO_2. By contrast, the global volume-averaged preformed nutrients are excellent indicators for atmospheric pCO_2.

3.1. Oceanic Circulation and Biological Export Production

[22] The simulated oceanic circulation relevant for the carbon cycle can be summarized as follows. Wind forces deep water rich in nutrients and *DIC* to upwell as Circumpolar Deep Water (CDW) to the south of the Antarctic Polar Front. The lower circulation (schematically shown in blue in Figure 1b) consists of the upwelling Southern Ocean water which moves southward and is subducted to the deep ocean south of the Polar Front as Antarctic Bottom Water (AABW). The upper circulation (in red in Figure 1b) comprises the upwelling Southern Ocean water which moves northward and eventually returns to the Southern Ocean via North Atlantic Deep Water (NADW).

[23] Changes in diapycnal diffusivity K_v and Southern Ocean winds have a large impact on both the lower and upper simulated circulations. As diapycnal diffusivity K_v increases, both the meridionally integrated zonal mass transport and the zonally integrated meridional mass transport increase [*Gnanadesikan et al.*, 2003] (Figures 2a–2b), resulting in stronger upper and lower circulations, i.e., stronger vertical exchange around 60°S and stronger sinking of dense water south of 60°S.

[24] Larger zonal wind magnitude at Drake Passage latitudes (55°S to 63°S) results in larger northward Ekman volume transport and forces stronger southward geostrophic flow at depth and more Southern Ocean upwelling in the windx3 compared to the LL run (Figures 2a and 2c). At the same time, stronger westerlies or stronger K_v drive an increase in Southern Ocean convective mixing (Figures 2d–2f). Since the overturning circulation is partly

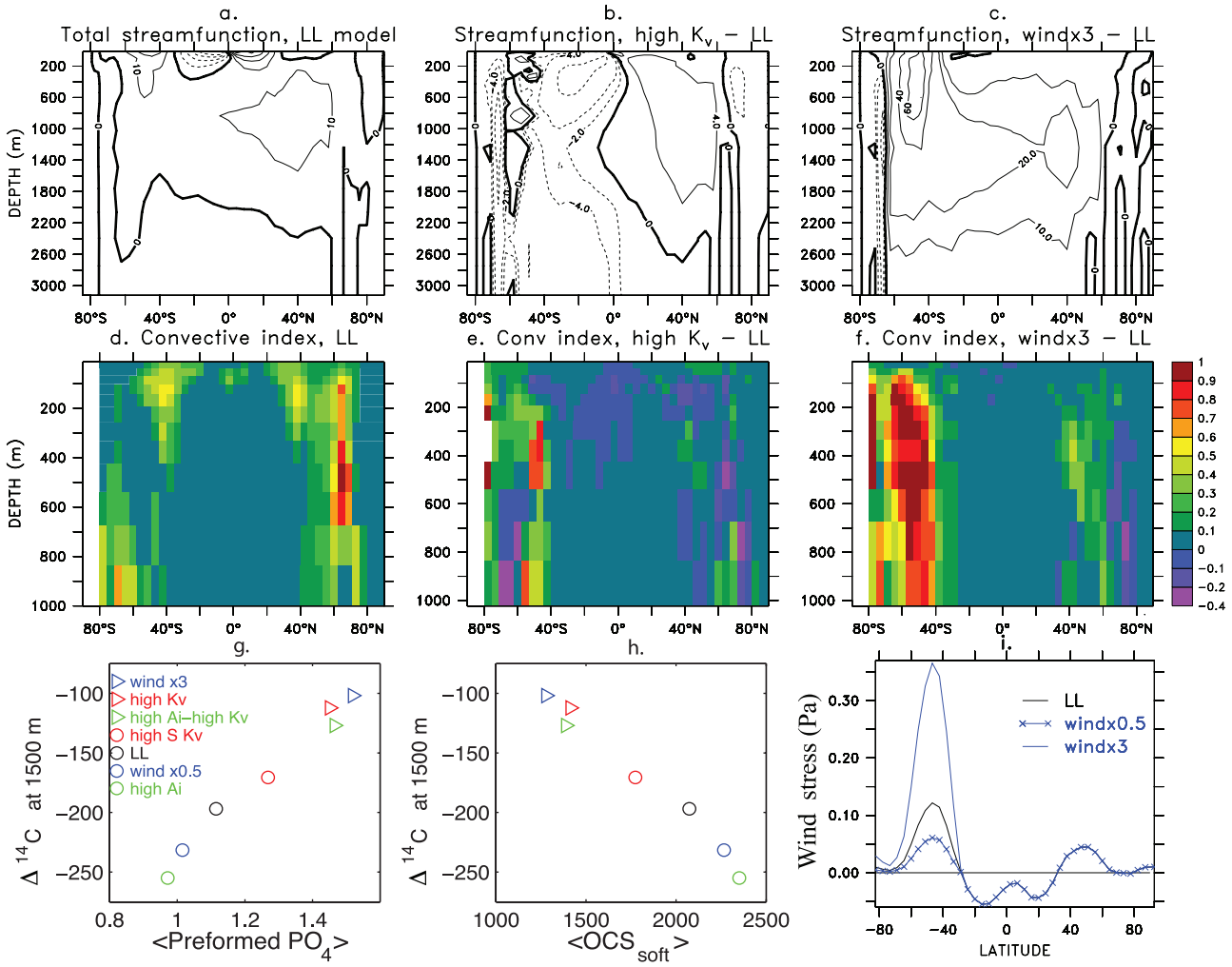

Figure 2. (a–c) Overturning streamfunction in Sv calculated as the zonal and depth integral of the meridional velocity for the LL model, high K_v − LL model difference, high Southern Ocean wind - LL difference. Shown streamfunctions are the sum between the GM and Euler streamfunctions. (d–f) Zonally averaged convective indices. Convective index is 1 when convection is on. A value of 0.5 can mean that half of the points at a given location are convecting all the time, that all points convect half of the time, or a scenario in between these two. (g–h) Covariation of $\Delta^{14}C$ (globally averaged at 1500 m) with globally averaged Preformed PO_4 (μmol/kg) and OCS_{soft} in the control simulations. The ocean carbon storage due to the soft-tissue pump (PgC) is calculated as $OCS_{soft} = V_{oc} \cdot r_{C:P} \cdot (\overline{PO_4} - \overline{PO_{4pref}})$. Deep waters in the high K_v and windx3 models are the youngest, best ventilated water masses while deep waters in the high A_i and windx0.5 models are oldest and least ventilated. Annual mean results are shown in all cases. (i) Annually and zonally averaged wind stresses for three of the models. Westerlies are positive.

driven by deep convection in the models, this results in a stronger lower-circulation cell and thus more vigorous deep ocean ventilation via the Southern Ocean.

[25] Examination of ^{14}C distributions show that the variations in deep ocean ^{14}C due to changes in winds or mixing emanate primarily from the Southern Ocean via AABW or convection. Less negative $\Delta^{14}C$ below the thermocline in both the high K_v and windx3 runs relative to the LL run indicates younger deep waters and more vigorous deepwater ventilation (Figure 2g). Conversely, smaller Southern Ocean winds or larger A_i result in a weaker Southern Ocean deep overturning cell and thus in less deepwater ventilation relative to the standard LL model, as indicated by more negative $\Delta^{14}C$ values.

[26] On the basis of our analysis of the oceanic circulation and ^{14}C in the models, we can broadly divide our models into low Southern Ocean ventilation models (LL, windx0.5, high A_i) and high Southern Ocean ventilation models (high K_v, high A_i-high K_v, windx2, windx3), depending on the strength of the Southern Ocean overturning or "lower" circulation.

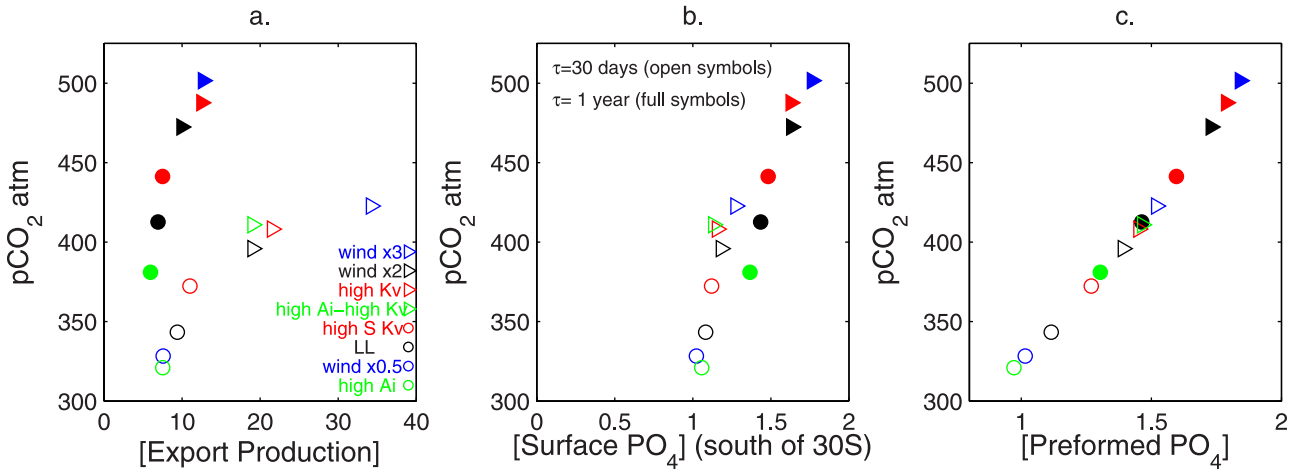

Figure 3. Atmospheric pCO_2 (ppm) versus (a) total globally averaged export Production (PgC/a), (b) average surface PO_4 south of 30°S (μmol/kg), and (c) global volume averaged preformed PO_4 (μmol/kg). Fast gas exchange simulations. Models have biological timescale τ = 30 days (open symbols) or τ = 1 year (full symbols). Shown are the LL (black circle), high A_i (green circle), windx0.5 (blue circle), high south K_v (red circle), high K_v-high A_i (green triangle) high K_v (red triangle), windx2 (black triangle), and windsx3 (blue triangle) models. Circles denote lower Southern Ocean ventilation models, and triangles denote higher-ventilation models.

[27] Oceanic circulation and convective mixing impact the distribution of biological export production (Figure 3a). Larger vertical mixing or larger Southern Ocean winds increase convection and upwelling of deep waters in Drake Passage latitudes. This implies a larger supply of deep ocean nutrients to the surface and higher global export production in the high mixing models relative to the standard (LL) model, with largest increases in convective regions such as the Weddell Sea. Conversely, lower Southern Ocean winds decrease convection and upwelling, slightly decreasing Southern Ocean biological production.

[28] Figure 3a shows that stronger biological export production is associated with higher pCO_{2a} and therefore with lower (not higher, as one might be tempted to think) oceanic accumulation of carbon across our seven models. Biological export production alone cannot be used to explain variations in pCO_{2a}. When biology is inefficient (τ = 1 year), a slow removal of surface PO_4 results in weaker export production and less pCO_{2a} drawdown compared to an efficient biology case (τ = 30 days; compare open and full symbols in Figure 3a). While the spread in export production is smaller when biology is inefficient, it is still the case that high-ventilation models have higher export production.

[29] Biological export production alone is not a good indicator for pCO_{2a} in our models. In order to understand atmospheric pCO_{2a} variations we need to understand what controls the CO_2 storage in the ocean.

3.2. Preformed and Remineralized Nutrients

[30] High surface nutrient concentrations, particularly in high latitudes, are a sign that biology is inefficient at these latitudes. The biologically unutilized nutrients which are subducted and transported into the interior ocean are called preformed nutrients.

[31] The total nutrient pool in the ocean can be divided into a preformed pool and a remineralized pool,

$$\overline{PO_4} = \overline{PO_{4\,pref}} + \overline{PO_{4\,remin}},$$

where an overline denotes global volume averages. Previous studies inferred preformed PO_4 from the concentration of apparent oxygen utilization or AOU:

$$PO_{4\,pref} = PO_4 - r_{O:P} \cdot AOU = r_{O:P} \cdot (O_2 - O_{2\,sat}),$$

where PO_4 and O_2 are model tracers and the saturation concentration $O_{2\ sat}$ is a function of local temperature and salinity. This method assumes that surface O_2 is in equilibrium with the atmosphere, an assumption which does not always hold and results in errors in AOU estimates [*Ito et al.*, 2004]. It is precisely to circumvent these problems that we introduce preformed PO_4 as an actual model tracer.

[32] Since surface preformed PO_4 is highest in the Southern Ocean, high Southern Ocean ventilation models (e.g., high K_v, windx3) have higher preformed phosphate concentration in the deep ocean compared to the low-ventilation models (LL, windx0.5, high A_i), as indicated by Figure 4 and by the nice $\Delta^{14}C - PO_{4\ pref}$ correlation (Figure 2g and Table 1).

[33] Remineralized nutrients are nutrients added to the ocean interior through organic matter remineralization, and are calculated here as the difference between two model tracers: total PO_4 and preformed PO_4. Since globally averaged total PO_4 is constant in our experiments, a smaller

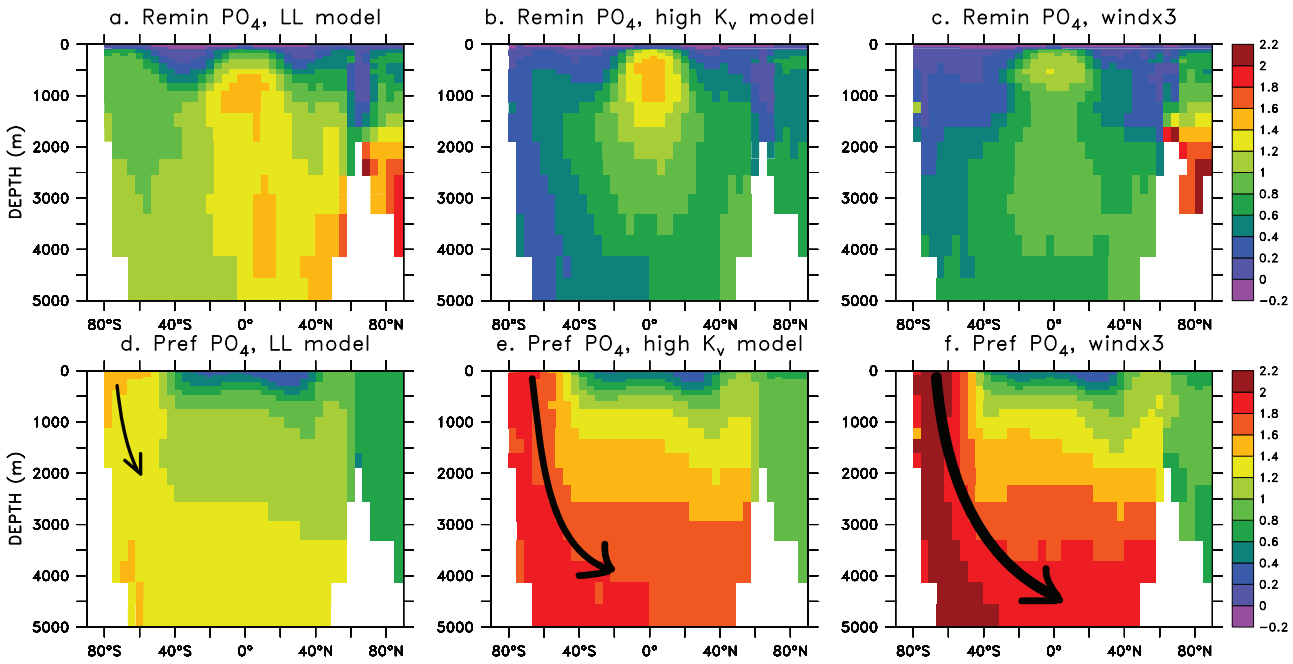

Figure 4. Global zonal averages of remineralized PO_4 (top) and preformed PO_4 (bottom) in the LL, high K_v and windx3 GCM simulations. Units are μmol/kg. Larger vertical mixing K_v or larger Southern Ocean winds result in stronger Southern Ocean overturning circulation (see arrows) and larger deep preformed PO_4.

nutrient fraction in the remineralized pool is equivalent to a larger nutrient fraction in the preformed pool and vice versa (Figures 4 and 5a–5b).

[34] Much oceanographic literature has been devoted to the connection between surface nutrients levels and atmospheric pCO_2 [e.g., *Archer et al.*, 2000]. Do we see a causal correlation between surface nutrients and pCO_{2a} in our GCMs?

[35] A cursory look at Figure 3b would seem to indicate a relationship between pCO_{2a} and surface nutrients. However, this is an indirect result of changes in circulation: higher vertical exchange results in more productivity which (because of our parameterization of productivity in terms of nutrient restoring) must be associated with higher surface nutrients. The idea that surface nutrient concentrations can be simply related to pCO_{2a} is undermined by the different linear relationships seen for the different restoring times. In the supplementary material (Text S1 and Figures S1 and S2) we present further evidence undermining the idea that there is a simple mapping from surface nutrients to pCO_{2a}, based on simulations in which the surface nutrients in the Southern Ocean are restored to zero.[1]

[36] By contrast, the global volume average of preformed PO_4 is an excellent indicator of pCO_{2a} (Figure 3c), with all simulations lying on a single line. In section 4.4 we ask whether intermodel changes in global preformed PO_4 are due to the observed changes in surface nutrients versus changes in ventilation, and conclude that the latter are critically important. We next analyze what determines the preformed $PO_4 - pCO_{2a}$ relationship.

4. Discussion

4.1. Ocean Carbon Storage, Preformed Nutrients and Atmospheric pCO_2: A Theoretical Analysis

[37] At every point in the ocean, *DIC* can be decomposed into its equilibrium contribution and components due to the soft-tissue, carbonate and solubility pumps:

$$DIC = DIC_{eq} + DIC_{soft} + DIC_{carb} + DIC_{solub} + DIC_{diseq}.$$

[38] In its most general form, the total amount of carbon in the atmosphere-ocean system can be written as

$$\begin{aligned} TC_{atm\,oc} &= M_{atm} \cdot pCO_{2\,a} + V_{oc} \cdot \overline{DIC} \\ &= M_{atm} \cdot pCO_{2\,a} + V_{oc} \cdot \overline{DIC_{eq}} + OCS_{soft} \\ &\quad + OCS_{carb} + OCS_{solub} + OCS_{diseq}, \end{aligned} \tag{2}$$

where M_{atm} is the mass of the atmosphere; V_{oc} is the ocean volume and overline denotes global volume average. The Ocean Carbon Storages due to the soft-tissue, carbonate and solubility pumps are $OCS_{soft} = V_{oc}\ DIC_{soft}$, $OCS_{carb} = V_{oc} \cdot DIC_{carb}$, $OCS_{solub} = V_{oc} \cdot DIC_{solub}$. The equilibrium (saturated) and the disequilibrium component of the carbon inventory are $V_{oc} \cdot \overline{DIC_{eq}}$ and $OCS_{diseq} = V_{oc}\ \overline{DIC_{diseq}}$.

[1] Auxiliary materials are available in the HTML. doi:10.1029/2007GB002958.

Table 1. Results From Eight Different Soft-Tissue Models[a]

Model	High Ai	windx0.5	Std (LL)	High South Kv	windx2	High Kv-High Ai	High Kv	windx3
$\Delta\ ^{14}C$	−254.7	−231.7	−196.7	−170.6	-	−127.0	−112.2	−101.9
$\overline{PO_{4pref}}$ (μmol/kg)	0.97	1.02	1.12	1.27	1.39	1.46	1.45	1.52
				Fast Gas Exchange				
$pCO_{2\ a}$ (ppm)	321.0	328.3	343.3	372.4	395.9	410.9	408.2	422.7
$M_a \cdot pCO_{2\ a}$ (ppm)	680.7	696.3	728.02	789.9	840.6	871.5	865.6	896.4
OCS_{soft} (PgC)	2350	2266	2072	1773	1534	1388	1413	1278
$V_{oc} \cdot \overline{DIC_{eq}}$ (PgC)	35433	35501	35635	35874	36050	36154	36136	36233
R	11.61	11.72	11.95	12.38	12.72	12.93	12.89	13.10
$C_{buffered}$ (PgC)	3733.8	3725.7	3710.4	3687	3674.3	3667	3667.9	3663.1
				Regular Gas Exchange				
$pCO_{2\ atm}$ (ppm)	288.3	294.2	299.0	329.2	335.3	361.2	352.8	356.2
$M_a \cdot pCO_{2\ atm}$(PgC)	611	624	635	698	711	766	748	755
OCS_{soft} (PgC)	2350	2266	2072	1773	1534	1388	1413	1278
OCS_{diseq} (PgC)	362	368	506	446	628	493	557	674
$V_{oc} \cdot \overline{DIC_{eq}}$ (PgC)	35011	35078	35126	35420	35463	35689	35617	35629

[a]Shown are global mean preformed PO_4, atmospheric pCO_2, and the terms in the air-sea carbon budget equation (equation (17)) for both fast gas exchange and regular gas exchange simulations. For the fast gas exchange simulations, the sum of OCS_{soft}, $M_{ac} \cdot pCO_{2atm}$, $V_{oc} \cdot [DIC_{eq}]$ equals 38,340 PgC for all models. Models are arranged in order of increasing deep ocean ventilation as measured by their mean ocean $\Delta\ ^{14}C$ at 1500 m. For the regular gas exchange simulations, the sum of the above three terms and of the disequilibrium component OCS_{diseq} equals 38,340 PgC. Note that the presence of surface disequilibrium changes both the atmospheric carbon budget and the oceanic equilibrium contribution. See also Figure 7 for a visual display of the different terms. Also shown for the fast gas exchange case are the Revelle Buffer factor R and the total buffered carbon in the ocean, $C_{buffered}$, defined in section 4.1.

[39] For a soft-tissue-only model in which surface CO_2 is in equilibrium with the atmosphere, the carbon inventory simplifies to

$$TC_{atm\,oc} = M_{atm} \cdot pCO_{2\,a} + V_{oc} \cdot \overline{DIC_{eq}} + OCS_{soft}. \tag{3}$$

[40] The total amount of remineralized carbon in the ocean due to the soft-tissue pump (OCS_{soft}) is exactly the remineralized PO_4 inventory scaled by a stoichiometric ratio:

$$\begin{aligned} OCS_{soft} &= r_{C:P} \cdot \overline{PO_{4\,remin.}} \cdot V_{oc} \\ &= r_{C:P} \cdot \left(\overline{PO_4} - \overline{PO_{4\,pref}}\right) \cdot V_{oc}, \end{aligned} \tag{4}$$

where V_{oc} is ocean volume and $r_{C:P} = 117$. As pointed out by *IF*, for a constant total ocean PO_4 (true by design in all our experiments), a decrease in global preformed PO_4 inventory results in an increase in global remineralized PO_4 inventory and in the ocean carbon storage. Disregarding for now the role of the equilibrium term, equation (3) suggests that a larger ocean carbon storage (and a smaller preformed PO_4), should result in smaller pCO_{2a}. Our model results demonstrate (Figures 5a–5c) that OCS_{soft}, the preformed PO_4 inventory and the remineralized PO_4 inventory all correlate well to pCO_{2a}. A high preformed PO_4 inventory means that there are low concentrations of remineralized phosphate and carbon in the deep ocean, low carbon storage and therefore high atmospheric pCO_2. Conversely, the oceanic carbon storage is at a maximum, and atmospheric pCO_2 is at a minimum, when all the nutrients in the deep ocean are in remineralized form and preformed nutrients are zero. In order to quantitatively predict the relationship between atmospheric pCO_2 and preformed nutrients, we now need to consider the role of the equilibrium term. Our theoretical analysis assumes that gas exchange at the ocean surface is infinitely fast; section 5 will comment on the role of disequilibrium.

[41] Let us perturb the system (equation (3)) by changing the soft-tissue pump. Since $TC_{atm\ oc}$ is assumed constant,

$$\begin{aligned} \delta TC_{atm\,oc} = M_a \cdot \delta pCO_{2\,a} + V_{oc} \cdot \delta\overline{DIC_{eq}} \\ + \delta OCS_{soft} = 0. \end{aligned} \tag{5}$$

[42] The goal is to find a simple relationship between pCO_{2a} and OCS_{soft}. The change in equilibrium carbon, $\delta\overline{DIC_{eq}}$, can be written as a function of the atmospheric carbon change, $\delta pCO_{2\,a}$. For each point at the ocean surface, the Revelle (buffer) factor is given by

$$R = \frac{\delta lnpCO_{2\,a}}{\delta lnDIC_{eq}}$$

[43] *IF* showed that to a good approximation one can replace DIC_{eq} above by its surface mean $\overline{DIC_{eq}}$ such that

$$R \simeq \frac{\delta lnpCO_{2\,a}}{\delta ln\overline{DIC_{eq}}} = \frac{\delta pCO_{2\,a}}{\delta\overline{DIC_{eq}}} \cdot \frac{\overline{DIC_{eq}}}{pCO_{2\,a}} \tag{6}$$

[44] We note that in our fast gas exchange models surface temperature and salinity are kept constant throughout the ocean for the purpose of the gas exchange calculation, such that equilibrium DIC is the same everywhere at the surface and (6) holds exactly. Replacing $\delta\overline{DIC_{eq}}$ from (6) in (5) we get

$$\frac{\delta pCO_{2\,a}}{\delta OCS_{soft}} = -\frac{pCO_{2\,a}}{M_a \cdot pCO_{2\,a} + V_{oc} \cdot \overline{DIC_{eq}}/R} \tag{7}$$

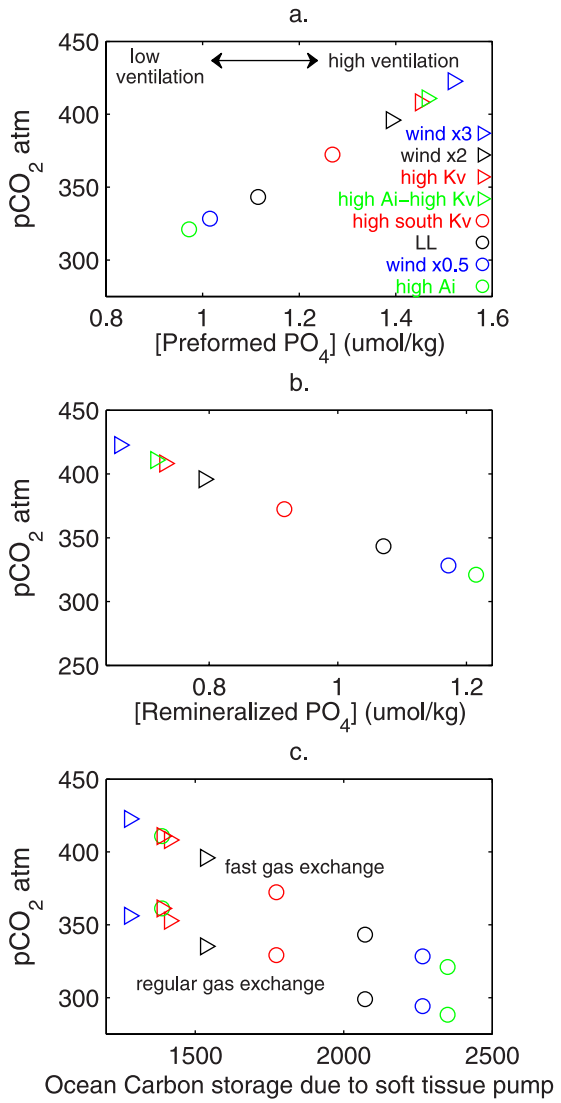

Figure 5. Atmospheric pCO_2 (ppm) versus (a) globally averaged preformed PO_4 (μmol/kg), (b) globally averaged remineralized PO_4 (μmol/kg), and (c) ocean carbon storage due to the soft-tissue pump (PgC) calculated as $OCS_{soft} = V_{oc} \cdot r_{C:P} \cdot ([PO_4] - [PO_{4\,pref}])$. Biological timescale τ = 30 days. Results in Figures 5a–5b are for fast gas exchange simulations. Figure 5c shows both fast gas exchange and regular gas exchange simulations.

[45] This equation was previously analyzed by *IF*, who proposed that for small changes in pCO_{2a} the right-hand side of the equation is approximately constant. With this assumption pCO_{2a} varies linearly with the soft-tissue carbon storage. Below we present a more accurate, exponential approximation to the differential equation (7).

4.1.1. New Exponential Approximation

[46] In a recent paper, *Goodwin et al.* [2007] suggested that under certain conditions the air-sea buffered carbon inventory, defined as "the total carbon inventory of the atmosphere plus the total buffered carbon inventory of the ocean" is approximately constant. Table 1 shows that their approximation holds reasonably well for the models presented in this paper. We note that

$$C_{buffered} = M_a \cdot pCO_{2\,a} + V_{oc} \cdot \frac{\overline{DIC_{eq}}}{R} \simeq constant,$$

holds in our models because as pCO_{2a} increases, R also increases in such a way as to restore $C_{buffered}$. The solution to (7) then becomes

$$pCO_{2\,a} \simeq c_1 \cdot e^{-\frac{OCS_{soft}}{C_{buffered}}} = c_1 \cdot e^{\frac{r_{C:P} \cdot \left(\overline{PO_{4\,pref}} - \overline{PO_4}\right) \cdot V_{oc}}{C_{buffered}}} \quad (8)$$

[47] This approximate solution holds since in our models, changes in the ratio $\frac{OCS_{soft}}{C_{buffered}}$ are dominated by changes in OCS_{soft}. The constant c_1 is the pCO_{2a} value for the limit in which OCS_{soft} = 0 and is 601 ppm for LL model. The exponential fit (8) approximates well the dependence of pCO_{2a} on OCS_{soft} observed in the model results (Figure 6).

4.1.2. Linear Approximation

[48] For small deviations in pCO_{2a} from a reference state, a Taylor series expansion of equation (8) gives

$$\begin{aligned} pCO_{2\,a} &\simeq c_2 - \frac{pCO_{2\,a\,ref}}{C_{buffered}} \cdot OCS_{soft} \\ &= c_2 - \frac{pCO_{2\,a\,ref}}{C_{buffered}} \cdot r_{C:P} V_{oc} \cdot \left(\overline{PO_{4\,pref}} - \overline{PO_4}\right) \end{aligned} \quad (9)$$

where c_2 is 537 ppm (LL model) and pCO_{2a} varies linearly with the ocean carbon storage. This formulation can be reconciled with the linear approximation proposed by *IF*.

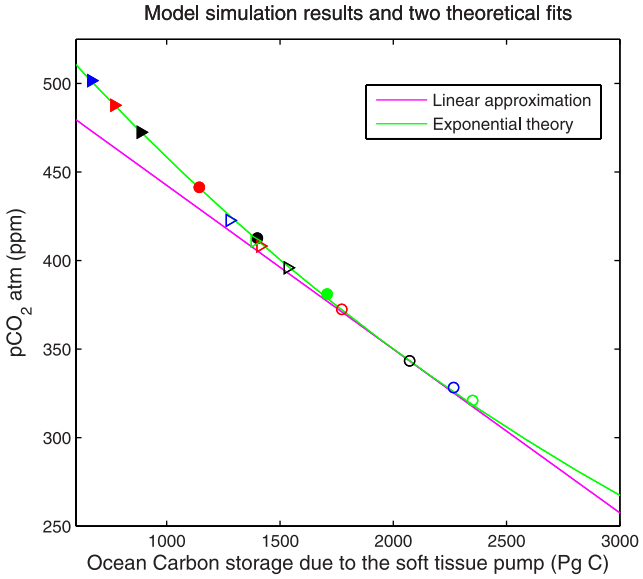

Figure 6. Variation of atmospheric pCO_2 (ppm) with the soft-tissue ocean carbon storage (PgC), $OCS_{soft} = V_{oc} \cdot r_{C:P} \cdot ([PO_4] - [PO_{4\,pref}])$. The exponential fit given by equation (8) and the linear fit given by equation (9) are shown on top of model results from eight different models. Fast gas exchange simulations shown for all models. Biological timescale τ is either 30 days (open symbols) or 1 year (full symbols). Model notation as in Figure 3.

[49] Figure 6 shows that equation (8) is a better fit than (9) to our model results. Follow-up work not shown here suggests that for large changes in ocean carbon storage (i.e., a broader spectrum of OCS_{soft} on the x axis of Figure 6), the exponential (8) holds increasingly better than the linear fit (9). Our results confirm that OCS_{soft}, which measures the ability of the soft-tissue pump to store CO_2 in the deep ocean, is the right norm for atmospheric pCO_2.

[50] Assuming that $\overline{PO_4}$ is constant, circulation-induced changes in global mean preformed PO_4 predict changes in pCO_{2a}. In the linear approximation,

$$\Delta pCO_{2\,a} \simeq \frac{pCO_{2\,a\,ref}}{C_{buffered}} \cdot r_{C:P} \cdot V_{oc} \cdot \Delta\overline{PO_{4\,pref}} = 179\frac{ppm}{\mu mol/kg} \cdot \Delta\overline{PO_{4\,pref}}(\mu mol/kg) \qquad (10)$$

where our reference point is the LL model and 179 is the linear slope in Figure 3c. A global increase in $\overline{PO_{4\,pref}}$ by 1 μmol/kg corresponds to a decrease in OCS_{soft} of 1935 PgC and an increase of about 179 ppm in pCO_{2a}.

4.2. What Controls Global Preformed Phosphate: Lessons From the Three-Box Model

[51] Having linked atmospheric pCO_2 to preformed nutrient, we now turn to the question of what controls preformed nutrient concentrations. The global preformed nutrient inventory is approximately given by the deep ocean preformed inventory. The three-box model (3BM) in Figure 1a offers us the most basic way of understanding what controls the deep preformed nutrients. Assuming zero low-latitude PO_4, the deep ocean and high-latitude preformed PO_4 values are identical:

$$Pref_d = Pref_h = PO_{4\,h},$$

where by definition the high-latitude surface preformed PO_4 equals the (total) PO_4 at the respective surface. Thus, in the three-box model, the only way to change the global integral of preformed nutrients is to change surface nutrients in the high-latitude box. One can analytically derive PO_{4h} as by *Sarmiento and Toggweiler* [1984, equation 9], such that

$$pCO_{2\,a} \propto Pref_d = PO_{4\,h} = \frac{M_{total} \cdot PO_{4\,total} - M_d \cdot Prod_h/f_{hd}}{M_h + M_d \cdot (1 + T/f_{hd})}, \qquad (11)$$

where M is the mass of a given reservoir; h and d are the high and deep ocean boxes, respectively; $Prod_h$ is the high-latitude export production; T is an advective term representing deepwater formation; and f_{hd} is mixing between the h and d boxes. The symbol $\propto$ shows, in the spirit of the linear approximation (9), that pCO_{2a} is proportional to the deep preformed PO_4 inventory.

[52] The 3BM suggested that changes in deep preformed nutrients and pCO_{2a} are driven entirely by changes in high-latitude surface nutrients, and inspired oceanographers to use surface nutrients as a metric for the biological pump impact on atmospheric pCO_2 [e.g., *Archer et al.*, 2000]. Surface nutrients in the high latitudes (and therefore deep preformed PO_4 and atmospheric pCO_2) depend very strongly on biological export production $Prod_h$ and f_{hd}.

[53] Let us assume $Prod_h$ is fixed in equation (11). Since f_{hd} supplies nutrients to the high-latitude surface, a larger f_{hd} increases PO_{4h} and deep preformed PO_4. A larger f_{hd} also brings more carbon from the deep, increasing surface CO_2 and outgassing more CO_2 to the atmosphere. This is consistent with the way the problem is often viewed in the paleoceanographic literature. Increased high-latitude stratification (smaller f_{hd}) is one of the classical hypotheses explaining the lower pCO_{2a} during glacials [e.g., *Francois et al.* 1997].

[54] Conversely, let us assume high-latitude mixing f_{hd} is fixed in equation (11). In this case there is a cause-effect relationship between biological production and pCO_{2a}. Larger export production results in smaller PO_{4h}, smaller $Pref_d$ and smaller atmospheric pCO_2. Intuitively this makes sense: larger export production lowers surface CO_2, allowing more CO_2 ingassing into the ocean and decreasing atmospheric pCO_2. This strong link implied by the 3BM resulted in much paleoceanographic work using biological export production as the implicit metric for the impact of biological pump on atmospheric pCO_2.

[55] Let us consider by comparison surface nutrients in our GCM suite. In our GCM we notice that

[56] 1. No unique functional relationship between surface PO_4 and pCO_{2a} can be established (see Figures 3b, S1, and S2). This contrasts with the exponential relationship found between global preformed PO_4 inventory and pCO_{2a} (Figure 3c). Unlike the 3BM, changes in surface nutrients (due to changes in mixing) explain at most half of the observed changes in deep preformed PO_4 and pCO_{2a} changes (section 4.4).

[57] 2. Higher export production is associated with higher pCO_{2a} (Figure 3a). This is contrary to the predictions of equation (11).

[58] Furthermore, *Marinov et al.* [2006] showed that global export production is controlled by the Subantarctic while atmospheric pCO_2 is controlled primarily by the Antarctic region of the Southern Ocean. This suggests that the link between pCO_{2a} and export production is much more complex than implied by a simple reading of equation (11). What mechanisms is the 3BM missing?

[59] A first clue is given by equation (11), which shows that high-latitude nutrients, and therefore atmospheric pCO_2, depend on the ratio $Prod_h/f_{hd}$. $Prod_h$ and f_{hd} have opposite effects on PO_{4h} and atmospheric pCO_2. This makes perfect physical sense: the surface CO_2 concentration depends both on export production ($Prod_h$), which acts to remove preformed nutrients and CO_2 from the surface, and on the vertical supply of nutrients and CO_2 to the ocean surface (f_{hd}). Furthermore, changes in high-latitude mixing affect biological production, such that $Prod_h$ and f_{hd} tend to be linked to each other. Thus, it is possible for larger $Prod_h$ not to be associated with smaller surface CO_2 if f_{hd} also changes.

[60] This is exactly what happens in our GCM. Larger K_v or Southern Ocean winds act to (1) increase f_{hd} and thus the supply of nutrients to the surface (which acts to increase

pCO_{2a}) and (2) increase biological export production $Prod_h$ (acting to decrease pCO_{2a}).

[61] From the point of view of pCO_{2a}, the first mechanism wins. Larger mixing or winds result in larger pCO_{2a} despite stronger export production. Changes in ocean circulation decouple pCO_{2a} from export production. We note however that in the absence of changes in ocean physics there would be a cause-effect relationship between the two variables, and larger export would mean lower pCO_{2a}.

[62] From the point of view of surface nutrients, the two mechanisms above balance closely and surface nutrients change little. Unlike the 3BM, we will show next that a significant percent of the observed change in pCO_{2a} in our GCMs cannot be explained by changes in surface PO_4. Sections 4.3–4.4 discuss an additional circulation mechanism, not present in a 3BM, which can explain the complex relationship between nutrients and pCO_{2a} observed in the GCM.

4.3. What Controls Global Preformed PO_4?: Lessons From the Four-Box Model

[63] Because the 3BM in Figure 1a allows only one way of forming deep water, deep preformed nutrients are entirely determined by surface nutrients in the high-latitude box. In the real ocean, preformed PO_4 is advected and mixed into the deep by the water masses which ventilate the deep ocean: AABW, NADW, Antarctic Intermediate Water and the Subantarctic Mode Water, the first two being the most important.

[64] To a good approximation, the ocean is dominated by a northern (T) and a southern source (f_{hd}), corresponding to the North Atlantic and Southern Ocean, respectively. Let us consider a four-box model (4BM) in which the generic high-latitude box is replaced by two distinct high-latitude boxes (Figure 1b). The net upwelling now takes place in the Southern Ocean, the net sinking in the North Atlantic.

[65] Since preformed PO_4 is conserved in the deep ocean, one can write

$$dPref_d/dt = (Pref_s - Pref_d)\cdot f_{hd} + T\cdot(Pref_n - Pref_d),$$

such that at steady state

$$pCO_{2\,a} \propto Pref_d = \frac{Pref_s\cdot f_{hd} + Pref_n\cdot T}{T + f_{hd}} = Pref_s - (Pref_s - Pref_n)\cdot\frac{T}{T+f_{hd}} \qquad (12)$$

[66] This is the equivalent of equation (11) for the 3BM. This equation shows clearly that the deep preformed nutrient concentration, a driver for pCO_{2a}, can be modified through changes in the relative contributions of the NADW (T) and AABW (f_{hd}) to the deep ocean. Significantly, a change in $Pref_d$ does not require a change in surface nutrients, as in the simpler 3BM.

[67] The net preformed PO_4 relevant for pCO_{2a} is now a linear combination of the surface preformed PO_4 in each deepwater formation area, weighted by the net ventilation of the deep reservoir by each water source. Since surface nutrients are higher in the Southern Ocean compared to the North Atlantic, $Pref_s - Pref_n > 0$. Assuming fixed $Pref_s$, $Pref_n$, and T, a larger southern ventilation rate f_{hd} results in a larger $Pref_d$ and higher pCO_{2a}.

Table 2. Preformed End-Members and Southern Ocean Ventilation in Four GCMs[a]

Model	$Pref_n$	$Pref_s$	$Pref_d$	f_s	$Pref_{surf\ S60S}$	$Pref_{surf\ S30S}$
High A_i	0.65	1.63	1.01	0.37	1.64	1.06
LL	0.70	1.66	1.20	0.52	1.67	1.08
High K_v	0.84	1.86	1.60	0.74	1.75	1.16
High A_i-high K_v	0.79	1.79	1.61	0.81	1.72	1.13

[a]Shown are the deep preformed PO_4 below 1500 m ($Pref_d$), the relative contribution of the Southern Ocean to the deep (f_s), surface preformed PO_4 south of 60°S ($Pref_{surf\ S60S}$), surface preformed PO_4 south of 30°S ($Pref_{surf\ S30S}$) for four models. End-members $Pref_s$ and $Pref_n$ are defined as the volume averages of preformed PO_4 south of 60°S and north of 40°N, respectively.

4.4. Analyzing Our GCM as a Four-Box Model

[68] As already noted, changes in circulation can both increase the surface nutrient concentrations and change the balance of waters ventilating the deep ocean. Which effect is most important in the GCMs? We begin our analysis by rewriting equation (12) as follows:

$$Pref_d = f_s\cdot Pref_s + f_n\cdot Pref_n \qquad (13)$$

where $f_s = f_{hd}/(T + f_{hd})$ and $f_n = T/(T + f_{hd})$ are the relative contributions of the Southern Ocean and North Atlantic, respectively, to the deep ocean.

[69] For a small circulation induced perturbation around a control state (e.g., the LL equilibrium state) and since $\Delta f_s = -\Delta f_n$ we approximate

$$\Delta Pref_d \simeq \Delta f_s\cdot\left(Pref_s^{ctrl} - Pref_n^{ctrl}\right) + \Delta Pref_s\cdot f_s^{ctrl} + \Delta Pref_n\cdot f_n^{ctrl} \qquad (14)$$

[70] Note that if we could somehow hold $Pref_s$ and $Pref_n$ fixed while f_s increased we would still see a $Pref_d$ increase. We now use equation (14) to evaluate which terms are most important in changing deep preformed phosphate in the GCMs. This task is nontrivial, since deepwater formation in our models happens seasonally in isolated convective areas. However, because we distinguish preformed and remineralized phosphate, we can isolate regions which have not had time to accumulate remineralized phosphate and are thus representative of the surface end-member. We defined $Pref_s$ as averaged preformed PO_4 everywhere south of 60° in waters where remineralized phosphate was less than 0.05 μmol/kg. $Pref_n$ was defined using the same conditions on the nutrients for the Atlantic basin north of 40°N. $Pref_s$ and $Pref_n$ are therefore the effective surface preformed nutrients as seen by the deep ocean. We note that $Pref_s$ is different from $Pref_{surf\ S60S}$, which is the preformed PO_4 averaged only over the Southern Ocean surface south of 60°S (Table 2).

[71] A simple analysis of four of our models is summarized in Table 2, where we calculate f_s on the basis of our end-member approximations and on equation (13). Table 3

Table 3. Processes Responsible for Changes in Deep Preformed PO_4[a]

	High A_i − LL	High K_v − LL	(High A_i-High K_v) − LL
$\Delta\ Pref_d$	−0.19	0.40	0.41
$\Delta f_s \cdot (Pref_s^{ctrl} - Pref_n^{ctrl})$	−0.15 (−80%)	0.211 (55%)	0.278 (79%)
$\Delta\ Pref_s \cdot f_s^{ctrl}$	−0.016 (−8%)	0.104 (27%)	0.067 (17%)
$\Delta\ Pref_n \cdot f_n^{ctrl}$	−0.024 (−12%)	0.067 (17%)	0.038 (10%)

[a]Units are μmol/kg. The terms in equation (14), comparing the LL model with three other models. Percents refer to contributions of the three terms on the right-hand side of equation (14) to $\Delta Pref_d$, and "ctrl" refers to the LL model values from Table 2. Most of the $Pref_d$ difference induced by subgrid-scale mixing can be ascribed to changes in f_s, the fraction of deep water of Southern Ocean origin. Increasing vertical mixing K_v increases f_s, which increases $Pref_d$ and atmospheric pCO_2. Increasing horizontal mixing A_i decreases f_s, $Pref_d$ and thus atmospheric pCO_2.

breaks the separate impacts of the changes in f_s, $Pref_s$ and $Pref_n$.

[72] We isolate the effect of vertical mixing by comparing the high-K_v model to the LL model. The increase in vertical mixing K_v increases the fraction of the deep water originating in the Southern Ocean (f_s) from 52% to 74%, a 42% increase. At the same time, the Southern Ocean preformed nutrients increase from 1.66 to 1.86 μmol/kg, a 12% increase. In Table 3, we calculate exactly the relative magnitudes of all terms in equation (14). Thus, we see that the increase in f_s accounts for 55% of the changes in $Pref_d$, while the increases in $Pref_s$ and $Pref_n$ account for 27% and 17%, respectively, of the $Pref_d$ change. Finally, we note that changes in $Pref_{surf\ S60S}$ are smaller than the changes in $Pref_s$. This shows that increasing vertical mixing in the ocean changes the deep ocean preformed PO_4 and therefore pCO_{2a} primarily through increasing the ventilation of the deep ocean via the Southern Ocean relative to the ventilation via NADW, equivalent to increasing f_{hd} in the 4BM.

[73] Changes in the isopycnal mixing coefficient A_i, which also corresponds to the so-called GM [*Gent and McWilliams*, 1990] coefficient, have a more complicated impact on atmospheric pCO_2. Larger A_i increases the Southern Ocean eddy overturning (which tends to decrease net residual mean overturning) and decreases convection [*Danabasoglu and McWilliams*, 1995; *Gnanadesikan et al.*, 2004]. In the models with low vertical mixing (LL and high A_i), increasing A_i results in a f_s drop from 0.52 to 0.37. Less deep ocean ventilation via the Southern Ocean implies less contribution of Southern Ocean nutrients to the deep ocean and smaller $Pref_d$. This results in more oceanic carbon storage and lower pCO_{2a}, as shown in Figure 5c, with the change in f_s accounting for 80% of the change in deep preformed nutrients. In the runs with high vertical mixing, by contrast, increasing A_i has a bigger impact on the northern overturning than on the southern overturning, so that f_s actually increases. This change in circulation is key to explaining why pCO_{2a} goes up in the high A_i-high K_v relative to the high-K_v model despite a decrease in surface preformed nutrients. Finally, comparing the high A_i-high K_v and LL models (right-hand column of Table 3). we see that circulation changes explain 79% of the difference in deep preformed nutrients.

[74] We do not claim that the direct effect of circulation changes in altering the mix of preformed waters is always more important than the indirect effect of changing the end-member preformed nutrient content. In fact, when we examined the impact of tripling the winds, we found that changes in f_s are less important than changes in end-member preformed nutrients. Nonetheless, changes in f_s (which varied from 0.42 to 0.55) still account for an important fraction of the changes in pCO_{2a} in these runs, with higher winds producing higher deep preformed nutrients and higher pCO_{2a}.

[75] Intuitively, our results make sense. Larger Southern Ocean winds or K_v result in larger vertical supply of CO_2 in the Southern Ocean through mixing or CDW upwelling. Because biology is highly inefficient in the Southern Ocean, much of this upwelled CO_2 escapes to the atmosphere, increasing atmospheric pCO_2. Conversely, an increase in eddy activity due to larger A_i results in less upwelling of CO_2 via the CDW and therefore lower atmospheric pCO_2.

[76] In summary, our GCM results show that one can have dramatic changes in deep preformed PO_4 and pCO_{2a} that cannot be fully accounted for by the smaller changes in mean surface nutrients (Figures 3b, 3c, S1, and S2). The presence of two deepwater formation regions effectively decouples deep preformed nutrients and pCO_{2a} changes from surface nutrient changes, as first observed by *Toggweiler* [1999]. Because it has only one deepwater formation region, the 3BM misses this mechanism. By contrast, a 4BM is the simplest box model that can allow the decoupling mechanism and can explain to first order our GCM results. In equations (13)–(14) one can change deep preformed PO_4 by changing f_s, even if surface preformed PO_4 does not change.

[77] The importance of oceanic circulation for atmospheric pCO_2 becomes clear when analyzing the terms in the atmosphere-ocean carbon inventory (equation (3)) for both the fast gas exchange and regular gas exchange simulations (Table 1 and Figure 7). For each model used the oceanic equilibrium component, V_{oc}*[DIC_{eq}], is about 17 times larger than OCS_{soft}, the next largest term, and about 50 times larger than the atmospheric carbon content. The atmospheric carbon content is only about 1.5–2% of the total air-sea carbon budget. In Figures 7a–7c and Table 1, models are arranged from left to right in order of increasing deepwater ventilation. As deep ventilation increases, deep preformed PO_4 increases and OCS_{soft} decreases. In fast gas exchange models, this decrease in soft-tissue carbon storage is exactly compensated by increases in both the carbon dioxide content of the atmosphere (Figure 7b) and in the equilibrium carbon content of the ocean (via an increase in surface *DIC*). In regular gas exchange models, circulation changes also induce changes in surface *DIC* disequilibrium, which in turn

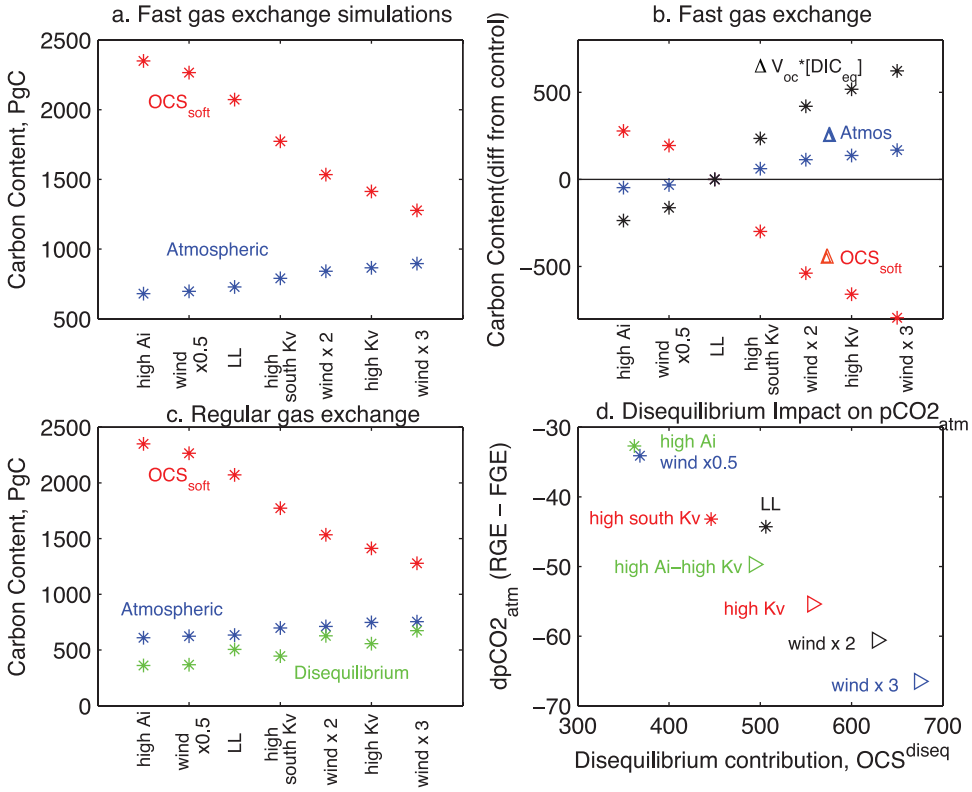

Figure 7. (a) Carbon budget contributions due to the atmosphere ($M_{atm} \cdot pCO_{2\,atm}$) and soft-tissue ocean carbon storage (OCS_{soft}) in the FGE simulations for seven of our models. Units are PgC. Oceanic equilibrium/saturation contribution not shown (about 20–50 times larger than the other components). Models arranged from left to right in order of increasing deepwater ventilation as indicated by $\Delta^{14}C$. (b) Carbon contributions - differences relative to the LL model for FGE simulations. Total air-sea carbon budget is identical for all models used. The change in OCS_{soft} relative to LL is compensated by changes in the atmospheric (blue) and oceanic equilibrium contributions (black). (c) Budget contributions in the RGE simulations. The ocean carbon storage due to surface disequilibrium (OCS_{diseq}) is smaller than all other components. (d) The decrease in atmospheric pCO_2 in ppm due to surface disequilibrium (i.e., the difference between regular and fast gas exchange pCO_2) plotted against the disequilibrium oceanic carbon storage from the RGE simulations, OCS_{diseq}, in PgC.

have an impact on atmospheric pCO_2. This disequilibrium is the topic for section 5.

5. Role of Surface CO_2 Disequilibrium in the Carbon Inventory

[78] The critical assumption in our discussion so far has been that CO_2 exchange at the ocean surface happens infinitely fast, such that CO_2 at the ocean surface is permanently in equilibrium with the atmosphere. Under this assumption, we concluded that the global preformed nutrient inventory determines the ocean biological carbon storage and atmospheric pCO_2.

[79] In reality, we know that CO_2 at the ocean surface takes about 9 months to equilibrate with the atmosphere, longer than typical mixed layer circulation timescales, such that CO_2 is out of equilibrium with the atmosphere. The degree of disequilibration depends on both the circulation timescale (which determines how fast CO_2 is upwelled, transported and downwelled) and on the biological timescale (at which biology incorporates carbon into organic matter).

[80] Let us consider a water parcel in a deepwater formation area with a disequilibrium contribution to its inorganic carbon content given by DIC_{diseq}. As the water parcel sinks into the deep ocean, it will continue to reflect the initial surface disequilibrium but it will also accumulate DIC from the soft-tissue pump, i.e., from the remineralization of organic matter through the water column. Disregarding the carbonate and the solubility pumps, DIC at each point in the ocean is the sum of the equilibrium, soft-tissue and disequilibrium components:

$$DIC = DIC_{eq} + DIC_{soft} + DIC_{diseq}. \tag{15}$$

[81] Since DIC_{diseq} is a conserved tracer in the ocean interior, we can write the deep ocean DIC_{diseq} by analogy with equation (13) as

$$DIC^{d}_{diseq} = DIC^{s}_{diseq} \cdot f_s + DIC^{n}_{diseq} \cdot f_n, \tag{16}$$

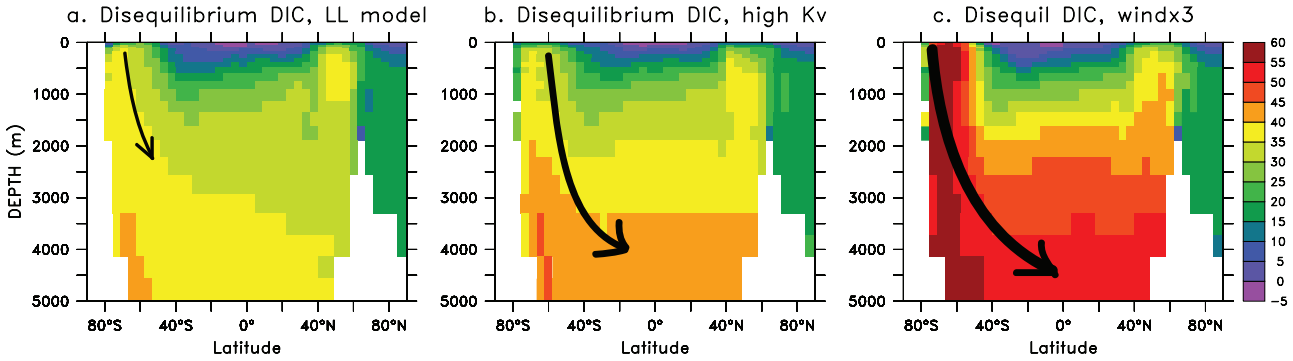

Figure 8. Global zonal averages of disequilibrium *DIC* in the (a) LL, (b) high K_v, and (c) windx3 GCMs. Results shown for the regular gas exchange (RGE) models. Disequilibrium *DIC* (μmol/kg) at each point calculated as the difference between total *DIC*, surface equilibrium *DIC*, and $DIC_{soft} = r_{C:P} \cdot (PO_4 - PO_{4\,pref})$. Increasing ventilation via the Southern Ocean results in more accumulation of deep disequilibrium *DIC*.

where DIC^s_{diseq}, DIC^n_{diseq}, DIC^d_{diseq} are the disequilibrium contributions of the Southern Ocean, North Atlantic and deep ocean. Deep ocean disequilibrium *DIC* is a linear combination of surface disequilibrium signatures modulated by the respective value of deep ocean ventilation. Is this 4BM picture reflected by the GCM results?

[82] Let us consider results from our regular gas exchange simulations in which surface CO_2 equilibration is slow. Figure 8 shows the zonally averaged disequilibrium *DIC* for the standard LL model, high K_v, and windx3 models with regular gas exchange. Disequilibrium *DIC* at each point in the ocean is calculated as the difference between total *DIC*, DIC_{eq}, and $DIC_{soft} = r_{C:P} \cdot (PO_4 - PO_{4\,pref})$.

[83] Upwelling and convection bring large quantities of CO_2 to the Southern Ocean surface. Slow gas exchange and a biology inefficient at taking up CO_2 result in a large positive Southern Ocean surface disequilibrium. This signal is subducted by the Southern Ocean lower circulation to the deep ocean. Larger K_v or Southern Ocean winds increase this circulation (f_s in equation (16)), and increase the positive average value of deep ocean DIC_{diseq}. Disequilibrium *DIC* is a useful tracer of oceanic circulation; its broad large-scale structure is similar to that of preformed PO_4 (compare Figures 8 and 4).

[84] The total carbon inventory of the atmosphere-ocean system becomes

$$\begin{aligned} TC_{atm\,oc} &= M_{atm} \cdot pCO_{2\,a} + V_{oc} \cdot \left(\overline{DIC_{eq}} + \overline{DIC_{soft}} + \overline{DIC_{diseq}}\right) \\ &= M_{atm} \cdot pCO_{2\,a} + OCS_{eq} + OCS_{soft} + OCS_{diseq}, \end{aligned} \quad (17)$$

where $OCS_{eq} = V_{oc} \cdot \overline{DIC_{eq}}$, $OCS_{soft} = V_{oc} \cdot r_{C:P}(\overline{PO_4^{3-}} - \overline{PO_{4\,pref}})$, and the oceanic carbon storage due to the surface disequilibrium is $OCS_{diseq} = V_{oc} \cdot \overline{DIC_{diseq}}$.

[85] Table 1 and Figures 7c–7d illustrate the terms in the above carbon budget for regular gas exchange simulations in our models. Though significant, the contribution of OCS_{diseq} to the total carbon inventory is smaller than the contribution of all other terms in equation (17) (Figure 7c). Consistent with Figure 8, the total ocean carbon content due to disequilibrium increases with larger vertical mixing K_v or stronger Southern Ocean winds. Conversely, larger isopycnal mixing A_i decreases the AABW formation and Southern Ocean convection. This decreases the contribution of Southern Ocean disequilibrium to the deep ocean, decreasing OCS_{diseq}.

[86] The impact of surface disequilibrium on atmospheric pCO_2 becomes clear when we compare results from the fast gas exchange or FGE simulations (instantaneous CO_2 surface equilibration, zero CO_2 disequilibrium) and regular gas exchange or RGE simulations (slow surface CO_2 equilibration, nonzero disequilibrium).

[87] Figure 5c shows oceanic carbon storage versus atmospheric pCO_2 in our eight circulation models. Changing the gas exchange equilibration timescale has a significant impact on atmospheric pCO_2 for a fixed ocean-atmosphere *DIC* inventory. Figure 5c shows that for a given circulation model (and therefore for a given biological pump and OCS_{soft}), the presence of disequilibrium considerably decreases pCO_{2a}.

[88] Water upwelling in the Southern Ocean brings large amounts of CO_2 from the deep. While in the FGE runs most of this CO_2 is instantaneously lost to the atmosphere, this is not the case in the RGE runs, where much of the additional CO_2 moves southward with the currents and is subducted to the deep. As a consequence, the presence of surface disequilibrium results in more ocean carbon storage and smaller atmospheric pCO_2 in the RGE compared to the FGE runs (Figures 5c, and 7d).

[89] To further complicate things, the impact of disequilibrium on pCO_2 varies among models with different circulations; it is −30 ppm in the windx0.5 and low A_i, −43 ppm in the LL and about −65 ppm in the windx3 model. The larger the oceanic carbon accumulation due to disequilibrium OCS_{diseq}, the smaller atmospheric pCO_2; the fit is almost linear (Figure 7d).

[90] Larger K_v or Southern Ocean winds result in a smaller OCS_{soft} (due to more accumulation of preformed PO_4 in the deep) and a larger OCS_{diseq} (due to more accumulation of DIC_{diseq} in the deep ocean). Surface CO_2 disequilibrium therefore interferes with the simple theoretical relationship between pCO_{2a} and OCS_{soft} derived in section 4.1. Our theoretical fit is not as good in the RGE

runs as in the FGE runs, and the slope of a linear fit is smaller in the former runs (Figure 5).

6. Conclusions

[91] This paper has focused on understanding in depth the mechanisms relating the soft-tissue pump and atmospheric pCO_2. Atmospheric pCO_2 is inversely related to the oceanic carbon storage which, in a soft-tissue-only model, is a simple function of the ocean preformed inventory. For a soft-tissue-only model with fast gas exchange we derive a simple exponential relationship between pCO_{2a} and the soft-tissue ocean carbon storage, OCS_{soft}. Our new theoretical fit compares favorably with model results and improves on the linear fit of *IF*. Further improvements on this theory are presented by *Marinov et al.* [2008].

[92] We have shown that the relative magnitudes of deepwater ventilation via the lower circulation (which includes AABW and Southern Ocean convection) and via NADW are critical in setting atmospheric pCO_2 because they impact the global preformed nutrients. Larger diapycnal mixing or stronger Southern Ocean winds considerably increase the deep ocean ventilation via the Southern Ocean and result in a larger fraction of deep ocean nutrients in the preformed pool, smaller oceanic carbon storage and higher atmospheric pCO_2. By contrast, increasing isopycnal mixing (in a weakly ventilated model) decreases the deep ocean ventilation via the Southern Ocean and decreases atmospheric pCO_2.

[93] Our findings agree with recent research demonstrating smaller atmospheric pCO_2 with reduced communication between Southern Ocean deepwater formation regions and the atmosphere, either through increased stratification [*Archer et al.*, 2003; *Gildor and Tziperman*, 2001; *Sigman and Boyle*, 2000; *Toggweiler*, 1999] or a shift in wind patterns [*Toggweiler et al.*, 2006].

[94] The relationship between pCO_{2a} and preformed PO_4 is complicated by the fact that surface CO_2 is out of equilibrium with the atmosphere. The impact of this disequilibrium on pCO_{2a} depends in a complex way on oceanic circulation. Future work should attempt to incorporate this disequilibrium signature in theoretical derivations.

[95] The present work shows that biological export production, usually associated in the literature with the strength of the biological pump, is not always a good predictor for atmospheric pCO_2. It is possible to have larger export with higher atmospheric pCO_2 in cases when both export and pCO_{2a} are affected by changes in ocean physics (which affect the supply rate of nutrients and carbon to the ocean surface).

[96] We have shown that the global inventory of preformed PO_4 is an excellent indicator for atmospheric pCO_2. By contrast, surface nutrients are not reliable predictors for atmospheric pCO_2 if oceanic circulation changes. In our model with simple OCMIP type biogeochemistry, we are able to produce large changes in atmospheric pCO_2 by changing oceanic circulation in such a way that the surface nutrient change is small, therefore effectively ''decoupling'' surface nutrients from atmospheric pCO_2. As first observed by *Toggweiler* [1999] and as discussed in the present paper, this decoupling does not happen in a three-box model but is present in a four-box model (and other more complicated models) of the ocean, which allow multiple deepwater sources. The extent of decoupling depends on the model circulation and on the parameterization of biological production. The decoupling must hold but might be weaker in a full ecological model.

[97] Deep ocean ventilation, and the related supply of preformed nutrients to the deep ocean, did not remain constant in the past and will likely change in the future. Without constraints on changes in circulation and nutrient supply, changes in export production or surface nutrients are not sufficient to explain changes in the total oceanic storage of carbon and in atmospheric pCO_2. Future studies that attempt to explain atmospheric pCO_2 changes must focus on changes in the preformed nutrient supply to the deep ocean.

[98] **Acknowledgments.** While at MIT, I.M. was supported by the NOAA Postdoctoral Program in Climate and Global Change, administered by the University Corporation for Atmospheric Research.

References

Archer, D. E., G. Eshel, A. Winguth, W. Broecker, R. Pierrehumbert, M. Tobis, and R. Jacob (2000), Atmospheric pCO_2 sensitivity to the biological pump in the ocean, *Global Biogeochem. Cycles*, *14*, 1219–1230.

Archer, D. E., P. A. Martin, J. Milovich, V. Brovkin, G. K. Plattner, and C. Ashendel (2003), Model sensitivity in the effect of Antarctic sea ice and stratification on atmospheric pCO_2, *Paleoceanography*, *18*(1), 1012, doi:10.1029/2002PA000760.

Broecker, W. S., and T. S. Peng (1992), *Tracers in the Sea*, 690 pp., Lamont-Doherty Geol. Lab., Columbia Univ., Palisades, N. Y.

Bryan, K., and L. J. Lewis (1979), A water mass model of the world ocean, *J. Geophys. Res.*, *84*, 2503–2517.

Danabasoglu, G., and J. C. McWilliams (1995), Sensitivity of the global ocean circulation to parameterizations of mesoscale tracer transports, *J. Clim.*, *8*, 2967–2987.

Francois, R. F., M. A. Altabet, E.-F. Yu, D. M. Sigman, M. P. Bacon, M. Frank, G. Bohrmann, G. Bareille, and L. D. Labeyrie (1997), Water column stratification in the Southern Ocean contributed to the lowering of glacial atmospheric CO_2, *Nature*, *389*, 929–935.

Gent, P. R., and J. C. McWilliams (1990), Isopycnal mixing in ocean circulation models, *J. Phys. Oceanogr.*, *20*(1), 150–155.

Gildor, H., and E. Tziperman (2001), Physical mechanisms behind biogeochemical glacial-interglacial CO_2 variations, *Geophys. Res. Lett.*, *28*, 2421–2424.

Gnanadesikan, A., R. D. Slater, N. Gruber, and J. L. Sarmiento (2002), Oceanic vertical exchange and new production: A comparison between models and observations, *Deep Sea Res., Part II*, *49*, 363–401.

Gnanadesikan, A., R. D. Slater, and B. L. Samuels (2003), Sensitivity of water mass transformation and heat transport to subgridscale mixing in coarse-resolution ocean models, *Geophys. Res. Lett.*, *30*(18), 1967, doi:10.1029/2003GL018036.

Gnanadesikan, A., J. P. Dunne, R. M. Key, K. Matsumoto, J. L. Sarmiento, R. D. Slater, and P. S. Swathi (2004), Oceanic ventilation and biogeochemical cycling: Understanding the physical mechanisms that produce realistic distributions of tracers and productivity, *Global Biogeochem. Cycles*, *18*, GB4010, doi:10.1029/2003GB002097.

Goodwin, P., R. G. Williams, M. J. Follows, and S. Dutkiewicz (2007), Ocean-atmosphere partitioning of anthropogenic carbon dioxide on centennial timescales, *Global Biogeochem. Cycles*, *21*, GB1014, doi:10.1029/2006GB002810.

Gruber, N., and J. L. Sarmiento (2002), Large-scale biogeochemical interactions in elemental cycles, in *The Sea*, vol. 12, edited by A. R. Robinson, J. J. McCarthy, and B. J. Rothschild, pp. 337–399, Wiley, J., New York.

Hellerman, S., and M. Rosenstein (1983), Normal monthly wind stress over the World Ocean with error estimates, *J. Phys. Oceanogr.*, *13*, 1093–1104.

Ito, T., and M. J. Follows (2005), Preformed phosphate, soft tissue pump and atmospheric CO_2, *J. Mar. Res.*, *63*(4), 813–839, doi:10.1357/0022240054663231.

Ito, T., M. J. Follows, and E. A. Boyle (2004), Is AOU a good measure of respiration in the oceans?, *Geophys. Res. Lett.*, *31*, L17305, doi:10.1029/2004GL020900.

Knox, F., and M. B. McElroy (1984), Changes in atmospheric CO_2: Influence of the marine biota at high latitude, *J. Geophys. Res.*, *89*, 4629–4637.

Louanchi, F., and R. G. Najjar (2000), A global climatology of phosphate, nitrate, and silicate in the upper ocean: Spring-summer export production and shallow remineralization, *Global Biogeochem. Cycles*, *14*, 957–977.

Marinov, I. (2005), Controls on the air-sea balance of carbon dioxide, Ph.D. thesis, Atmos. and Oceanic Sci. Program, Princeton Univ., Princeton, N. J.

Marinov, I., A. Gnanadesikan, J. R. Toggweiler, and J. L. Sarmiento (2006), The Southern Ocean biogeochemical divide, *Nature*, *441*, 964–967, doi:10.1038/nature04883.

Marinov, I., M. Follows, A. Gnanadesikan, J. L. Sarmiento, and R. D. Slater (2008), How does ocean biology affect atmospheric pCO_2?: Theory and models, *J. Geophys. Res.*, doi:10.1029/2007JC004598, in press.

Najjar, R., et al. (2007), Impact of circulation on export production, dissolved organic matter, and dissolved oxygen in the ocean: Results from Phase II of the Ocean Carbon-Cycle Model Intercomparison Project (OCMIP 2), *Global Biogeochem. Cycles*, *21*, GB3007, doi:10.1029/2006GB002857.

Pacanowski, R. C., and S. M. Griffies (1999), *The MOM3 Manual, Alpha Version*, 580 pp., NOAA/Geophys. Fluid Dyn. Lab. Princeton, N. J.

Sarmiento, J. L., and J. R. Toggweiler (1984), A new model for the role of the oceans in determining atmospheric pCO_2, *Nature*, *308*, 620–624.

Siegenthaler, U., and T. H. Wenk (1984), Rapid atmospheric CO_2 variations and ocean circulation, *Nature*, *308*, 624–626.

Sigman, D. M., and E. A. Boyle (2000), Glacial/interglacial variations in atmospheric carbon dioxide, *Nature*, *407*, 859–869.

Toggweiler, J. R. (1999), Variation of atmospheric CO_2 by ventilation of the ocean's deepest water, *Paleoceanography*, *14*, 571–588.

Toggweiler, J. R., R. Murnane, S. Carson, A. Gnanadesikan, and J. L. Sarmiento (2003), Representation of the carbon cycle in box models and GCMs: 2. Organic pump, *Global Biogeochem. Cycles*, *17*(1), 1027, doi:10.1029/2001GB001841.

Toggweiler, J. R., J. L. Russell, and S. R. Carson (2006), Mid-latitude westerlies, atmospheric CO_2 and climate change during the ice ages, *Paleoceanography*, *21*, PA2005, doi:10.1029/2005PA001154.

Trenberth, K. E., J. Olson, and W. Large (1989), A global ocean winds stress climatology based on ECMWF Analyses, *Tech. Rep. NCAR/TN-338+STR*, Natl. Cent. for Atmos. Res., Boulder, Colo.

Volk, T., and M. I. Hoffert (1985), Ocean carbon pumps: Analysis of relative strengths and efficiencies in ocean driven atmospheric CO_2 changes, in *The Carbon Cycle and Atmospheric CO_2: Natural Variations Archaean to Present, Geophys. Monogr. Ser.*, vol. 32, edited by E. T. Sundquist and W. S. Broecker, 99–110, AGU, Washington, D. C.

M. Follows, Program in Atmospheres, Oceans, and Climate, Massachusetts Institute of Technology, 54-1412, 77 Massachusetts Avenue, Cambridge, MA 02139, USA. (mick@plume.mit.edu)

A. Gnanadesikan and J. R. Toggweiler, NOAA/Geophysical Fluid Dynamics Laboratory, P. O. Box 308, 201 Forrestal Road, Princeton, NJ 08542, USA. (anand.gnanadesikan@noaa.gov; robbie.toggweiler@noaa.gov)

I. Marinov, Department of Marine Chemistry and Geochemistry, Woods Hole Oceanographic Institution, MS 25, 360 Woods Hole Road, Woods Hole, MA 02543, USA. (imarinov@whoi.edu)

B. K. Mignone, The Brookings Institution, 1775 Massachusetts Avenue NW, Washington, DC 20036, USA. (bmignone@brookings.edu)

J. L. Sarmiento, Atmospheric and Oceanic Sciences Program, Princeton University, Sayre Hall, Forrestal Campus, P. O. Box CN710, Princeton, NJ 08544, USA. (jls@princeton.edu)